Geophysical Research Letters

RESEARCH LETTER
10.1029/2018GL080940

Global Meridional Overturning Circulation Inferred From a Data-Constrained Ocean & Sea-Ice Model

Sang-Ki Lee[1], Rick Lumpkin[1], Molly O. Baringer[1], Christopher S. Meinen[1], Marlos Goes[1,2], Shenfu Dong[1], Hosmay Lopez[1,2], and Stephen G. Yeager[3]

[1]NOAA Atlantic Oceanographic and Meteorological Laboratory, Miami, FL, USA, [2]Cooperative Institute for Marine and Atmospheric Studies, University of Miami, Miami, FL, USA, [3]National Center for Atmospheric Research, Boulder, CO, USA

Key Points:
- The global meridional overturning circulation is revisited using an ocean model with its T&S corrected and validated against observations
- Several underexplored aspects are highlighted, including complex but vigorous heavy-to-light water conversion in the Indo-Pacific Ocean
- Key processes including deep water formation & heavy-to-light water conversion are poorly captured in a model without T&S corrections

Supporting Information:
- Supporting Information S1

Correspondence to:
S.-K. Lee,
sang-ki.lee@noaa.gov

Citation:
Lee, S.-K., Lumpkin, R., Baringer, M. O., Meinen, C. S., Goes, M., Dong, S., et al. (2019). Global meridional overturning circulation inferred from a data-constrained ocean & sea-ice model. *Geophysical Research Letters*, *46*, 1521–1530. https://doi.org/10.1029/2018GL080940

Received 16 OCT 2018
Accepted 11 DEC 2018
Accepted article online 18 DEC 2018
Published online 2 FEB 2019

Abstract Our current understanding of the global meridional overturning circulation (GMOC) is revisited using a surface-forced ocean model simulation constrained by global hydrographic data. The derived GMOC is qualitatively consistent with previous observation-based studies and further provides enhanced spatial details in the sources, transformations, and transports of major global water masses including in poorly observed regions. Several important but relatively underexplored aspects of the GMOC are highlighted, including complex but vigorous heavy-to-light water mass transformation that occurs in the Indo-Pacific and Southern Oceans, and the role of the equatorial Pacific upwelling in closing the GMOC circuit. These and other key aspects of the GMOC are poorly captured in a surface-forced ocean model simulation without the temperature and salinity corrections, suggesting that current climate models do not realistically simulate the GMOC and the associated global heat, salt, and carbon balances.

Plain Language Summary Ocean tracers such as heat, salt, and carbon are perpetually carried by the global meridional overturning circulation (GMOC) and redistributed between hemispheres and across ocean basins from their source regions. The GMOC is therefore a crucial component of the global heat, salt, and carbon balances. In order to better understand the GMOC, here we carry out a global ocean model simulation with its temperature and salinity corrected toward observations. The derived GMOC is presented, validated against observations, and summarized in a schematic, which highlights several important but relatively underexplored aspects of the GMOC, including the pathway through which the heaviest water mass formed around the Antarctica is brought to the surface. This and other key aspects of the GMOC are poorly captured in a model run without the temperature and salinity corrections, suggesting that current climate models do not reproduce realistic paths of the GMOC and the associated global heat, salt, and carbon balances.

1. Introduction

The global meridional overturning circulation (GMOC), often referred to as the ocean conveyor belt, is a large-scale ocean circulation system that connects the Arctic, Atlantic, Indian, and Pacific Oceans via the Southern Ocean. It is predominantly driven by deep convection in the high-latitude North Atlantic Ocean and around the Antarctica, wind-driven upwelling in the Southern Ocean (e.g., Broecker, 1987, 1991; Gordon, 1986a, 1986b; Schmitz, 1995; Talley, 2013) and abyssal diapycnal mixing (Munk & Wunsch, 1998). The GMOC carries heat, salt, carbon, and other biogeochemical elements along its paths, redistributing them between hemispheres and across ocean basins, and thus is a crucial component of the global heat, salt, and carbon balances (e.g., Evans et al., 2017; Macdonald & Wunsch, 1996; Sarmiento & Le Quere, 1996; Talley, 2003, 2008).

Hydrographic section data collected during repeated cruises have been used to estimate the GMOC (e.g., Ganachaud, 2003; Ganachaud & Wunsch, 2000; Hernández-Guerra & Talley, 2016; Lumpkin & Speer, 2007; Sloyan & Rintoul, 2001; Talley, 2003). Lumpkin and Speer (2007, LS07 hereafter), for example, applied inverse techniques to World Ocean Circulation Experiment hydrographic sections together with current measurements and air-sea heat and freshwater fluxes to present a schematic view of the GMOC circuit, which is widely considered to be an up-to-date view. Their estimates, however, are subject to large spatio-temporal sampling errors inherent in the one-time synoptic World Ocean Circulation Experiment

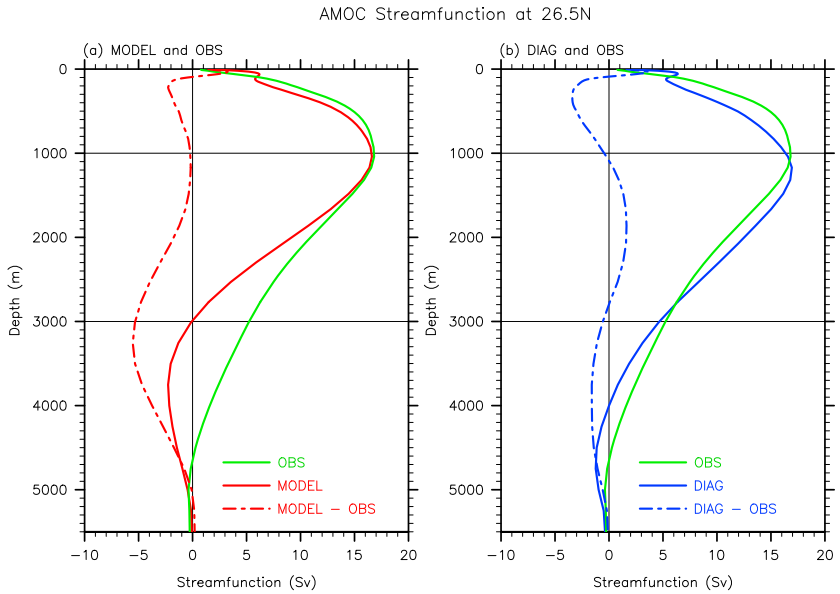

Figure 1. The AMOC stream functions at 26.5°N derived from (a) a surface-forced ocean & sea-ice simulation (MODEL) and (b) a robust diagnostic simulation (DIAG), in reference to RAPID-MOC/MOCHA/WBTS array observations (OBS). Volume transports are in Sverdrup (10^6 m^3/s) units. AMOC = Atlantic meridional overturning circulation.

hydrographic sections. For instance, the hydrographic sections used in LS07 were collected predominantly during summer months in the 1990s. Additionally, only two global composite zonal transects at 32°S and 62°S were available to estimate the overturning circulations in the South Indian, South Pacific, and Southern Oceans. As such, some aspects of the GMOC are still poorly understood. For example, the heaviest water mass formed around the Antarctica, known as Antarctic Bottom Water (AABW), must be transformed into a much lighter water mass to close the GMOC circuit (e.g., Talley, 2013). However, it is still not entirely clear through what paths AABW is brought near to the surface. With sustained monitoring programs such as RAPID-MOC/MOCHA/WBTS (Cunningham et al., 2007), SAMBA (Meinen et al., 2018), and OSNAP (Lozier et al., 2017), the paths of the GMOC in the Atlantic Ocean are relatively well studied compared to those in the Southern and Indo-Pacific Oceans. However, in spite of a relative abundance of observations, previous studies do not agree on exactly how much of North Atlantic Deep Water (NADW) is formed in the Greenland, Iceland, and Norwegian (GIN) Seas versus in the Labrador and Irminger Seas (e.g., Lumpkin & Speer, 2003; Smethie & Fine, 2001) or the relative proportions of the northward flowing surface and intermediate depth waters entering the South Atlantic Ocean (Schmitz, 1995). Therefore, there still remain many open questions and large spatiotemporal gaps to fill to achieve a more comprehensive understanding of the GMOC.

Global atmosphere-ocean (and ocean-only) general circulation models (GCMs) are often used to fill the gaps in the observation-based estimates and also to understand the related ocean processes. However, current generation GCMs suffer from several critical systematic biases in the GMOC. For example, the Atlantic meridional overturning circulation (AMOC), the Atlantic component of the GMOC, observed at 26.5°N by the RAPID-MOC/MOCHA/WBTS array is characterized by the southward returning flow extending from about 1,000 m to the ocean floor near 5,000 m (Figure 1a). A surface-forced ocean & sea-ice model, on the other hand, shows a much shallower southward returning flow between about 1,000 and 3,700 m (Figure 1a)—this model is described in section 2. This shallower southward flow in turn transports excessive heat southward (Danabasoglu et al., 2014, 2016) and thus produces colder-than-observed sea surface temperatures in the Northern Hemisphere (Wang et al., 2014). This is a common symptom in the majority of surface-forced ocean & sea-ice models participating in Coordinated Ocean-ice Reference Experiments phase 2 as well as in many fully coupled models participating in the Coupled Model Intercomparison Project phase 5 (Danabasoglu et al., 2014, 2016). This and other limitations in current generation GCMs undermine our ability to better understand and describe the GMOC. Therefore, in order to minimize the known limitations in GCMs, here we utilize a surface-forced ocean & sea-ice model simulation constrained by long-term averaged

global hydrographic data—this technique is often referred to as a robust diagnostic simulation in the literature (e.g., Sarmiento & Bryan, 1982).

The overarching goal of this study is to fill spatiotemporal gaps in the GMOC derived from previous observation-based estimates. As a first step toward achieving this goal, here we revisit our current understanding of the GMOC by using a robust diagnostic simulation and validating it against previous observation-based studies. In the following sections, after a brief description of the data, model, and robust diagnostic simulation used (section 2), we compare the AMOC profile at 26.5°N between model runs with and without the temperature and salinity corrections, in reference to the RAPID-MOC/MOCHA/WBTS array observations. Good agreement between the robust diagnostic simulation and the observations allows us to further investigate the flow paths of the GMOC in the Atlantic, Indo-Pacific, and Southern Oceans using the robust diagnostic simulation (section 3). The GMOC derived from a model run without the temperature and salinity corrections is also presented (section 3), followed by a discussion on some important discrepancies in the GMOC between this and previous studies (section 4). Finally, the GMOC derived from the robust diagnostic simulation is summarized in a schematic (section 5), which is qualitatively consistent with most previous observation-based studies (e.g., LS07; Talley, 2013), and further provides enhanced spatial details in the sources, transformations, and transports of the major global water masses.

2. Data, Model, and Robust Diagnostic Simulation

In an effort to reconstruct realistic flow paths of the GMOC, we performed an ocean & sea-ice model simulation with its temperature and salinity relaxed toward long-term averaged global hydrographic observations. This method, known as robust diagnostic simulation, corrects baroclinic geostrophic velocities throughout the water column and also improves the representations of surface heat and fresh water fluxes. As such, robust diagnostic simulation has been successfully used to reconstruct ocean currents in the Atlantic Ocean (e.g., Bogden et al., 1993; Ezer & Mellor, 1994; Greatbatch et al., 1991; Sarmiento & Bryan, 1982; Wright et al., 2006). However, robust diagnostic simulation has not previously been applied globally to study the GMOC outside of the Atlantic basin. See supporting information Text S1 for further discussion about robust diagnostic simulation.

We used the ocean & sea-ice model components of the National Center for Atmospheric Research (NCAR) Community Earth System Model version 1 (CESM1; Danabasoglu et al., 2012) forced with the European Center for Medium-Range Weather Forecasts (ECMWF) twentieth century reanalysis (Poli et al., 2016) surface flux fields. The CESM1 ocean and sea-ice model was initialized using January temperature and salinity fields obtained from the Polar Hydrographic Climatology (Steele et al., 2001) and spun up for 300 years using the ECMWF twentieth century reanalysis surface flux fields. The surface flux fields in each model year were randomly selected from the period of 1948–1977, following the time-shuffling spin-up method used in Lee et al. (2011, 2017).

During the spin-up run, to prevent the model temperature and salinity fields from drifting away from the observed climatology, the global temperature and salinity fields were slowly relaxed to the World Ocean Atlas 2013 version 2 climatology (Locarnini et al., 2013; Zweng et al., 2013) with an e-folding time of 5 years. The World Ocean Atlas 2013 version 2 climatology used is a combination of monthly temperature and salinity fields in the upper 2,000 m and annual mean fields below 2,000 m. The spin-up run was continued for an additional 100 years, which is referred to as DIAG hereafter and used to describe the GMOC. In addition, we performed the same model simulation without the temperature and salinity relaxations for 1,000 years. The last 100 years of this simulation is referred to as MODEL hereafter and compared with DIAG in the following sections. See Text S1 for more detailed descriptions about the CESM1 ocean & sea-ice model and the sensitivity of the model solutions to the relaxation time.

3. Atlantic Meridional Overturning Circulation at 26.5°N in Depth Coordinate System

Figures 1a and 1b show the AMOC stream functions at 26.5°N derived from MODEL and DIAG, respectively, compared to the RAPID-MOC/MOCHA/WBTS array observations (OBS hereafter). The maximum AMOC at this latitude is about 17 Sv in both MODEL and DIAG, consistent with OBS (e.g., Smeed et al., 2018). However, the southward return flow compensates for the northward flow at about 3,000 m in MODEL compared to about 4,700 m in OBS (zero-crossings in Figure 1a). This suggests that in MODEL,

the formation of the lower NADW (i.e., through deep convection in the GIN Seas and subsequent overflows) and its southward excursion throughout the Atlantic basin are far too weak, whereas the formation of the upper NADW (i.e., through deep convection in the Labrador and Irminger Seas) and its southward transport are too strong. Additionally, the AMOC stream function in MODEL continues to decrease down to around 3,700 m and then increases thereafter, indicating that significant northward spreading of AABW occurs below 3,700 m. However, such a large northward flow of AABW at 26.5°N is not supported in OBS (Hernández-Guerra et al., 2014; McCarthy et al., 2015; Smeed et al., 2018).

As shown in Figure 1b, the southward transport between 1,000 and 3,000 m agrees much better between DIAG (12.0 Sv) and OBS (11.9 Sv). The southward transport below 3,000 m also agrees well (4.6 Sv in DIAG; 4.9 Sv in OBS). Some discrepancies between DIAG and OBS are still noted. For example, the depth of the maximum AMOC is shifted downward by about 200 m in DIAG with respect to OBS. Nevertheless, the vertical AMOC profile in DIAG is overall in much better agreement with OBS compared to MODEL, especially in the southward return flow below 1,000 m.

Given a good agreement of the AMOC profile at 26.5°N between DIAG and OBS, we further analyze the GMOC for the Atlantic, Indo-Pacific, and Southern Oceans derived from DIAG and validate it against observation-based estimates from LS07 and others in the following sections. However, it is important to realize that using a depth range to define a water mass is in general misleading because the depth range for a given water mass changes at different locations. Therefore, in order to better describe the sources and detailed paths of the GMOC, we use potential density as the vertical coordinate system.

4. GMOC in Density Coordinate System

4.1. Atlantic Ocean

Figures 2a and 2b show the zonally integrated overturning stream function in the Southern Ocean (south of 35°S) and in the Atlantic Ocean (north of 35°S) derived from DIAG. The vertical axis is potential density referenced to 2,000 m (i.e., in σ_2 units). Tracing the stream function contours allows us to compute the transport of water masses in classes defining surface water, intermediate depth water, and NADW. The surface water ($\sigma_2 < 35.7$) is known to originate largely from the Indian Ocean via the Agulhas leakage (e.g., Beal et al., 2011; Gordon, 1986a). It is carried northward below the surface mixed layer and brought to the surface via the equatorial Atlantic upwelling. At 26.5°N, about 10.2 Sv of the warm surface water is transported northward (Figure 2c). Antarctic Intermediate Water (AAIW) that forms at the surface mixed layer in the southeast Pacific is an important source of intermediate depth water ($\sigma_2 = 35.7$–36.8; e.g., McCartney, 1977; Talley, 1996). However, AAIW begins to lose its well-distinguishable minimum salinity signature as it moves northward across the equator (e.g., Talley, 2013). At 26.5°N, the northward transport of intermediate depth water is about 6.9 Sv (Figure 2c). Eventually, the surface and intermediate depth water masses sink into the deeper ocean through deep convection at high latitudes.

Two distinctive sinking regions are readily identifiable. One is centered at around 60–65°N where the lighter portion of NADW (i.e., upper NADW, $\sigma_2 = 36.8$–37.1) is formed, mainly in the Labrador and Irminger Seas. The other is located north of around 70°N where heavier NADW (i.e., lower NADW, $\sigma_2 > 37.1$) is formed, mainly in the GIN Seas. In total, about 17.1 Sv of NADW is carried southward through the AMOC return flow across 26.5°N (i.e., transport below $\sigma_2 > 36.8$). Although there is no clear stream function boundary that separates upper and lower NADW away from the formation regions, tracing the stream function back to the formation areas indicates that outflow of dense water formed in the GIN Seas entrains lighter water to form lower NADW. It appears that lower NADW originating from the GIN Seas and upper NADW formed in Labrador and Irminger Seas contribute roughly equally to the southward return flow of the AMOC (i.e., 7.7 and 9.4 Sv, respectively, at 26.5°N, Figure 2c). Smethie and Fine (2001) estimated lower NADW formation rate of about 7.5 Sv and upper NADW formation rate of about 9.6 Sv, which are very close to our estimates. LS07 estimated the southward NADW transport of 16.8 ± 2.3 Sv at 48°N, which is also consistent with our result of 17.1 Sv at 26.5°N. The southward transport of NADW is nearly uniform in terms of both magnitude and vertical profile throughout the Atlantic Ocean southward of 26.5°N, which is overall consistent with the observation-based estimates by LS07 (16.9 Sv at 30°S in DIAG; 17.6 ± 3.7 Sv at 32°S in LS07) and others (e.g., 17.9 ± 2.2 Sv at 34.5°S in Dong et al., 2009; 18.1 ± 2.3 Sv at 35°S in Garzoli et al., 2013).

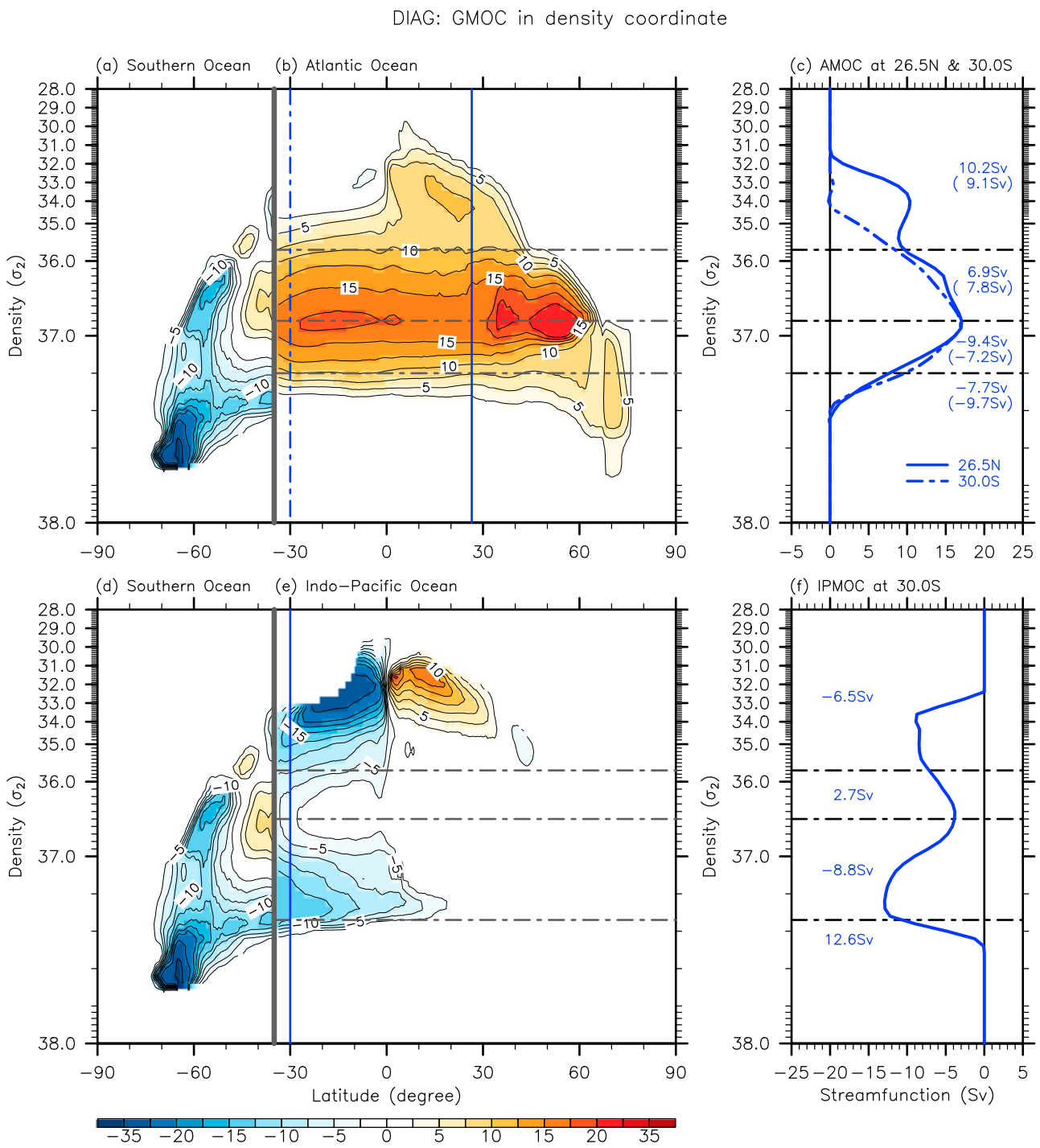

Figure 2. The GMOC in (a and d) the Southern Ocean (south of 35°S), in (b) the Atlantic Ocean (north of 35°S), and in (e) the Indo-Pacific Ocean (north of 35°S); (c) the AMOC at 26.5°N (solid line) and 30.0°S (dashed line); and (f) the IPMOC at 30.0°S, derived from DIAG. The vertical axis is potential density in reference to 2,000 m (1,000 kg/m^3 is subtracted from the potential density to produce σ_2 units). The AMOC transport values for the surface water ($\sigma_2 < 35.7$), intermediate depth water ($\sigma_2 = 35.7$–36.8), upper North Atlantic Deep Water ($\sigma_2 = 36.8$–37.1), and lower North Atlantic Deep Water ($\sigma_2 > 37.1$) are shown for 26.5°N and 30.0°S (in parentheses) in (c). The IPMOC transport values for the surface water ($\sigma_2 < 35.7$), Antarctic Intermediate Water ($\sigma_2 = 35.7$–36.5), Indian Deep Water and Pacific Deep Water ($\sigma_2 = 36.5$–37.17), and Antarctic Bottom Water ($\sigma_2 > 37.17$) are shown for 30.0°S in (f). Volume transports are in Sverdrup units. IPMOC = Indo-Pacific meridional overturning circulation; AMOC = Atlantic meridional overturning circulation; GMOC = global meridional overturning circulation.

4.2. Southern and Indo-Pacific Oceans

Figures 2a and 2b show that the southward flow of NADW into the Southern Ocean is the major source of the local water mass in the Southern Ocean known as Circumpolar Deep Water (CDW). Largely driven by wind-induced upwelling, CDW carries high salinity NADW close to the surface in the Southern Ocean (Gnanadesikan, 1999; Marshall & Speer, 2012; Toggweiler & Samuels, 1998). Lower NADW, in particular, is the major source of lower CDW that eventually sinks near the Antarctica (mainly in the Weddell and Ross Seas) to form AABW. As shown in Figure 2a, the magnitude of the overturning circulation associated with AABW formation exceeds 35 Sv south of 65°S. However, the closed stream function lines indicate that a large portion of the southern overturning cell recirculates within the Southern Ocean, and only about 12.7 Sv is exported out of the Southern Ocean across 35°S, which is close to the AABW contribution to the GMOC (14 Sv) by Orsi et al. (2002), but smaller than other observation-based estimates at around 32°S (46.0 $\pm$ 1.0 Sv in Sloyan & Rintoul, 2001; 20.9 $\pm$ 6.7 Sv in LS07; 21.0 in Ganachaud, 2003; 22.0 Sv in Talley, 2013).

Figures 2d and 2e show the overturning circulations in the Southern Ocean (south of 35°S) and in the Indo-Pacific Oceans (north of 35°S). AABW forms near the Antarctica, becomes lighter north of 60°S, and then is exported into the Indo-Pacific Oceans. At 30°S, about 12.6 Sv of AABW ($\sigma_2 > 37.17$) is exported into the Indo-Pacific Oceans (Figure 2f), which is smaller than 15.3 $\pm$ 5.1 Sv at 32°S estimated by LS07. The abyssal water mass that enters the Indo-Pacific Oceans ultimately transforms into Indian Deep Water and Pacific Deep Water (PDW; $\sigma_2 = 36.5 \sim 37.17$) through diapycnal mixing (e.g., Talley, 2013). A smaller portion of PDW directly supplies cold and fresh water to the equatorial Pacific upwelling (3.8 Sv). Indian Deep Water and the rest of PDW flow back into the Southern Ocean (8.8 Sv at 30°S) to form upper CDW, which also originates to a lesser degree from upper NADW in the South Atlantic (Figures 2a and 2b). Upper CDW in part transforms into AAIW ($\sigma_2 = 35.7–36.5$) in the surface-mixed layer in the southeast Pacific and is transported back into the Atlantic and Indo-Pacific Oceans (e.g., Talley, 2013). Cold and fresh AAIW (2.7 Sv) is carried northward below the South Pacific subtropical cell and subsequently brought to the surface via the equatorial Pacific upwelling (6.5 Sv). This complex but vigorous heavy-to-light water mass transformation from AABW to surface water is a key step to close the GMOC circuit. It is qualitatively in line with the observation-based schematic views of LS07 and Talley (2013) and further shows that the equatorial Pacific upwelling is an important player in completing the heavy-to-light water mass transformation.

4.3. MODEL

As shown in Figure 3, some key aspects of the GMOC described above are poorly captured in MODEL. For example, the southward return flow of the AMOC in MODEL originates predominantly from the Labrador and Irminger Seas, while outflow of dense water formed in the GIN Seas contributes very little. NADW at 35°S is also much lighter than lower CDW at that latitude, indicating a weak linkage between the two compared to DIAG. Additionally, much less and heavier abyssal water enters the Indo-Pacific Ocean from the Southern Ocean in MODEL compared to DIAG. But, most importantly, the heavy-to-light water mass transformation in the Indo-Pacific and Southern Oceans, which is a critical component to close the GMOC circuit, is almost completely missing in MODEL.

5. Discussions

The GMOC derived from DIAG provides enhanced spatial details in the sources, transformations, and transports of major global water masses in regions not sampled by the hydrographic sections used in LS07 and Talley (2013). As such, some aspects of the GMOC shown in Figures 2 and 3 cannot be verified against observations. For instance, our analysis indicates that upper CDW, which enters the Pacific Ocean as AAIW, and intermediate depth water sourced directly from PDW are carried northward beneath the South Pacific subtropical cell and subsequently brought to the surface via the equatorial Pacific upwelling. This intricate water mass transformation pathway is generally in line with a water mass balance between two hydrographic sections at 28°S and 24°N (Talley, 2008, 2013) and further shows that the equatorial Pacific upwelling is an important player in the heavy-to-lighter water transformation from AABW to surface water. However, more hydrographic sections within the tropical Pacific are required to verify this pathway.

Another potentially important aspect that has not been resolved in observations is a recirculation of the southern meridional overturning cell. The maximum transport of this cell exceeds 35 Sv, from which

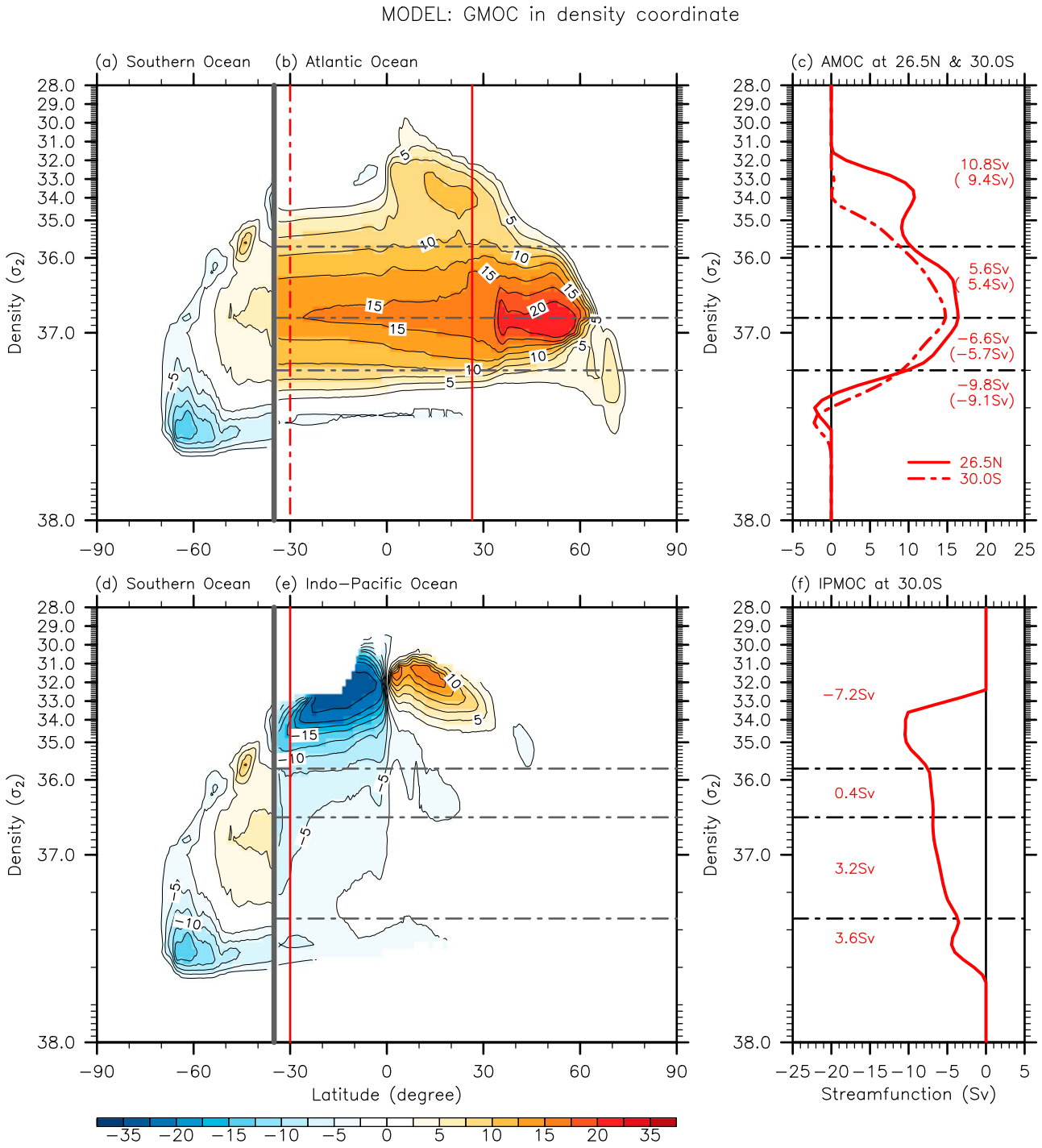

Figure 3. Same as Figure 2 but derived from MODEL. IPMOC = Indo-Pacific meridional overturning circulation; AMOC = Atlantic meridional overturning circulation; GMOC = global meridional overturning circulation.

about two thirds recirculate within the Southern Ocean near the Antarctica and only about 12.7 Sv is carried northward across 35°S after mixing with lighter water. Previous observation-based studies, on the other hand, estimated that about 21–46 Sv of AABW is formed near the Antarctica and carried across around 32°S with little or no recirculation (Ganachaud, 2003; LS07; Sloyan & Rintoul, 2001; Talley, 2003, 2013). Farneti et al. (2015) showed that some surface-forced ocean models display a similar recirculation cell in the Southern Ocean and attributed it to a local recirculation of the subpolar gyres in the Weddell and

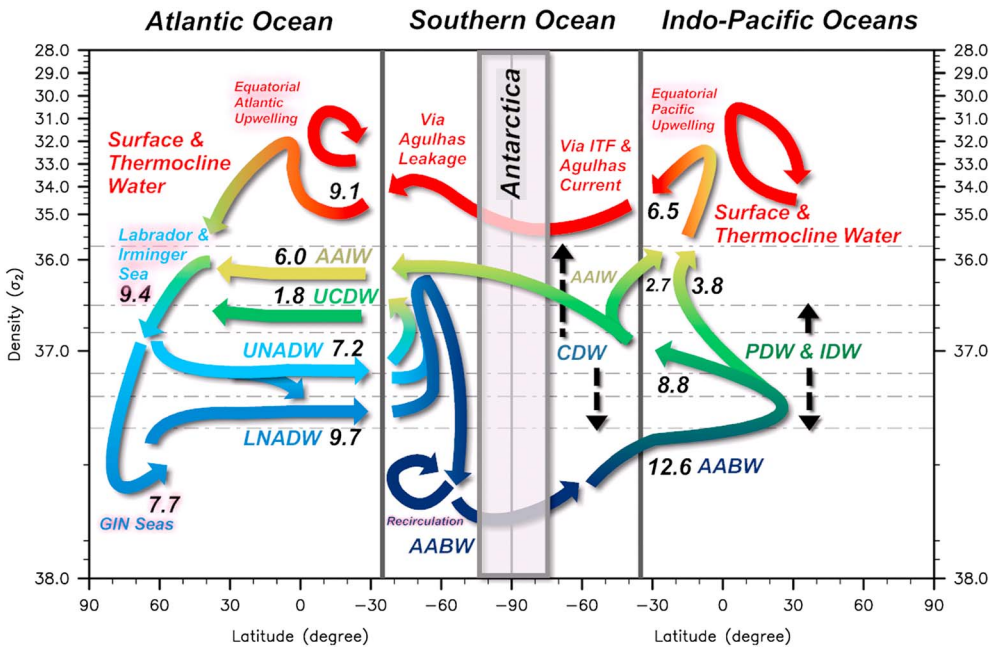

Figure 4. A summary schematic of the global meridional overturning circulation as discussed in the text. Color indicates approximate density ranges of the water masses involved. Volume transports are in Sverdrup units. Black-dotted lines indicate the density ranges of CDW, IDW, and PDW. Specific components that are not resolved in the observation-based schematic views of LS07 and Talley (2013) are highlighted with red background color. AAIW = Antarctic Intermediate Water; AABW = Antarctic Bottom Water; GIN = Greenland, Iceland, and Norwegian; CDW = Circumpolar Deep Water; PDW = Pacific Deep Water; IDW = Indian Deep Water; LNADW = Lower North Atlantic Deep Water; UNADW = Upper North Atlantic Deep Water; UCDW = Upper Circumpolar Deep Water.

Ross Seas. Although currently there is no observational evidence for its existence, a recirculation of the southern meridional overturning cell has important implications for the regional heat and mass balance. Thus, future observational efforts are needed.

It is important to point out that there are some noticeable differences between DIAG and the observations presented by LS07 and others. For example, LS07 estimated that 5.6 ± 3.0 Sv of AABW spreads northward across 32°S into the Atlantic Ocean, which is eventually transformed into lower NADW and exported back to the Southern Ocean. This is also supported by other observational studies (e.g., Johnson, 2008). In DIAG, however, the net northward transport into the South Atlantic below NADW nearly vanishes. Further analysis is needed to explore what causes the near-absence of the AABW transport into the South Atlantic. This and other shortcomings in DIAG may be reduced in the future if an eddy-resolving ocean & sea-ice model (e.g., Maltrud & McClean, 2005) is used to better represent eddy-driven ocean transports, inertial boundary currents, and topography-induced mixing. A systematic evaluation of the restoring terms in DIAG in reference to the parameterized mixing terms may also be useful (e.g., Arzel & Colin de Verdière, 2016).

6. Summary

We revisited our current understanding of the GMOC by using a model-based reconstruction of the GMOC that is qualitatively consistent with most previous observation-based studies across the key hydrographic sections. A summary schematic of the GMOC is shown in Figure 4, which highlights several important aspects of the GMOC that were not resolved in the observation-based schematic views of LS07 and Talley (2013). First, the equatorial Pacific upwelling system plays an important role in completing the heavy-to-light water mass transformation from AABW to surface water. Second, outflow of dense water mass from the GIN Seas entrains lighter water to form lower NADW, which in turn contributes to roughly half of the southward return flow of the AMOC. Third, a large portion of the southern overturning cell may recirculate within the Southern Ocean. Fourth, the equatorial Atlantic upwelling serves as an important cross-hemispheric pathway through which the South Atlantic surface water originating from the Indian Ocean

is carried to the deep convection sites in the North Atlantic. Finally, these and other key aspects of the GMOC derived from DIAG are poorly captured in a surface-forced ocean model simulation without the temperature and salinity corrections, which suggests that current generation climate models have limitations in simulating the GMOC and the associated global heat, salt, and carbon balances. See Text S2 for an extended summary of Figure 4.

Acknowledgments
We would like to sincerely thank three anonymous reviewers and Janet Sprintall for their insightful comments and suggestions, which led to a significant improvement of the paper. We also would like to thank Young-Oh Kwon for kindly providing a MATLAB code that converts CESM1 output into density coordinate. S.-K. Lee acknowledges George Halliwell for helpful comments and suggestions. ERA-20C surface flux data were provided by ECMWF at http://www.ecmwf.int. The World Ocean Atlas 2013 version 2 climatology data were provided by NOAA's National Centers for Environmental Information at http://www.nodc.noaa.gov. The RAPID-MOC/MOCHA/WBTS AMOC monitoring data at 26.5°N were provided by the RAPID-WATCH MOC monitoring project website at https://www.rapid.ac.uk/rapidmoc. This work was supported by NOAA's Climate Program Office, Climate Variability and Predictability Program (award GC16-207) and NOAA's Atlantic Oceanographic and Meteorological Laboratory.

References

Arzel, O., & Colin de Verdière, A. (2016). Can we infer diapycnal mixing rates from the World Ocean temperature–salinity distribution? *Journal of Physical Oceanography*, *46*(12), 3751–3775. https://doi.org/10.1175/JPO-D-16-0152.1

Beal, L. M., De Ruijter, W. P., Biastoch, A., Zahn, R., Cronin, M., Hermes, J., et al. (2011). On the role of the Agulhas system in ocean circulation and climate. *Nature*, *472*(7344), 429–436. https://doi.org/10.1038/nature09983

Bogden, P. S., Davis, R. E., & Salmon, R. (1993). The North Atlantic circulation: Combining simplified dynamics with hydrographic data. *Journal of Marine Research*, *51*(1), 1–52. https://doi.org/10.1357/0022240933223855

Broecker, W. S. (1987). The biggest chill. *Natural History Magazine*, *97*, 74–82.

Broecker, W. S. (1991). The Great Ocean conveyor. *Oceanography*, *4*(2), 79–89. https://doi.org/10.5670/oceanog.1991.07

Cunningham, S. A., Kanzow, T., Rayner, D., Baringer, M. O., Johns, W. E., Marotzke, J., Longworth, H. R., et al. (2007). Temporal variability of the Atlantic meridional overturning circulation at 26.5°N. *Science*, *317*(5840), 935–938. https://doi.org/10.1126/science.1141304

Danabasoglu, G., Bates, S. C., Briegleb, B. P., Jayne, S. R., Jochum, M., Large, W. G., et al. (2012). The CCSM4 ocean component. *Journal of Climate*, *25*(5), 1361–1389. https://doi.org/10.1175/JCLI-D-11-00091.1

Danabasoglu, G., Yeager, S. G., Bailey, D., Behrens, E., Bentsen, M., Bi, D., et al. (2014). North Atlantic simulations in coordinated ocean-ice reference experiments phase II (CORE-II). Part I: Mean states. *Ocean Modelling*, *73*, 76–107. https://doi.org/10.1016/j.ocemod.2013.10.005

Danabasoglu, G., Yeager, S. G., Kim, W. M., Behrens, E., Bentsen, M., Bi, D., et al. (2016). North Atlantic simulations in coordinated ocean-ice reference experiments phase II (CORE-II). Part II: Inter-annual to decadal variability. *Ocean Modelling*, *97*, 65–90. https://doi.org/10.1016/j.ocemod.2015.11.007

Dong, S., Garzoli, S. L., Baringer, M. O., Meinen, C. S., & Goni, G. J. (2009). Interannual variations in the Atlantic meridional overturning circulation and its relationship with the net northward heat transport in the South Atlantic. *Geophysical Research Letters*, *36*, L20606. https://doi.org/10.1029/2009GL039356

Evans, G. R., McDonagh, E. L., King, B. A., Bryden, H. L., Bakker, D. C. E., Brown, P. J., et al. (2017). South Atlantic interbasin exchanges of mass, heat, salt and anthropogenic carbon. *Progress in Oceanography*, *151*, 62–82. https://doi.org/10.1016/j.pocean.2016.11.005

Ezer, T., & Mellor, G. L. (1994). Diagnostic and prognostic calculations of the North Atlantic circulation and sea level using a sigma coordinate ocean model. *Journal of Geophysical Research*, *99*(C7), 14,159–14,171. https://doi.org/10.1029/94JC00859

Farneti, R., Downes, S. M., Griffies, S. M., Marsland, S. J., Behrens, E., Bentsen, M., et al. (2015). An assessment of Antarctic Circumpolar Current and Southern Ocean meridional overturning circulation during 1958–2007 in a suite of interannual CORE-II simulations. *Ocean Modelling*, *93*, 84–120. https://doi.org/10.1016/j.ocemod.2015.07.009

Ganachaud, A. (2003). Large-scale mass transports, water mass formation, and diffusivities estimated from World Ocean Circulation Experiment (WOCE) hydrographic data. *Journal of Geophysical Research*, *108*(C7), 3213. https://doi.org/10.1029/2002JC001565

Ganachaud, A., & Wunsch, C. (2000). Improved estimates of global ocean circulation, heat transport and mixing from hydrographic data. *Nature*, *408*(6811), 453–457. https://doi.org/10.1038/35044048

Garzoli, S., Baringer, O., Dong, S., Perez, R. C., & Yao, Q. (2013). South Atlantic meridional fluxes. *Deep Sea Research Part I*, *71*, 21–32. https://doi.org/10.1016/j.dsr.2012.09.003

Gnanadesikan, A. (1999). A simple predictive model for the structure of the oceanic pycnocline. *Science*, *283*(5410), 2077–2079, https://doi.org/10.1126/science.283.5410.2077

Gordon, A. L. (1986a). Interocean exchange of thermocline water. *Journal of Geophysical Research*, *91*(C4), 5037–5,046, https://doi.org/10.1029/JC091iC04p05037

Gordon, A. L. (1986b). Is there a global scale ocean circulation? *Eos, Transactions American Geophysical Union*, *67*(9), 109–110. https://doi.org/10.1029/EO067i009p00109

Greatbatch, R. J., Fanning, A. F., & Goulding, A. D. (1991). A diagnosis of interpentadal circulation changes in the North Atlantic. *Journal of Geophysical Research*, *96*(C12), 22009–22023. https://doi.org/10.1029/91JC02423

Hernández-Guerra, A., Pelegrí, J. L., Fraile-Nuez, E., Benítez-Barrios, V., Emelianov, M., Pérez-Hernández, M. D., & Vélez-Belchí, P. (2014). Meridional overturning transports at 7.5 N and 24.5 N in the Atlantic Ocean during 1992–93 and 2010–11. *Progress in Oceanography*, *128*, 98–114. https://doi.org/10.1016/j.pocean.2014.08.016

Hernández-Guerra, A., & Talley, L. D. (2016). Meridional overturning transports at 30° S in the Indian and Pacific Oceans in 2002–2003 and 2009. *Progress in Oceanography*, *146*, 89–120. https://doi.org/10.1016/j.pocean.2016.06.005

Johnson, G. C. (2008). Quantifying Antarctic Bottom Water and North Atlantic Deep Water volumes. *Journal of Geophysical Research*, *113*, C05027. https://doi.org/10.1029/2007JC004477

Lee, S.-K., Park, W., van Sebille, E., Baringer, M. O., Wang, C., Enfield, D. B., et al. (2011). What caused the significant increase in Atlantic Ocean heat content since the mid-20th century? *Geophysical Research Letters*, *38*, L17607. https://doi.org/10.1029/2011GL048856

Lee, S.-K., Volkov, D., Lopez, H., Cheon, W. G., Gordon, A. L., Liu, Y., & Wanninkhof, R. (2017). Wind-driven ocean dynamics impact on the contrasting sea-ice trends around West Antarctica. *Journal of Geophysical Research: Oceans*, *122*, 4413–4430. https://doi.org/10.1002/2016JC012416

Locarnini, R. A., Mishonov, A. V., Antonov, J. I., Boyer, T. P., Garcia, H. E., Baranova, O. K., et al. (2013). In S. Levitus, & A. Mishonov (Eds.), *World Ocean Atlas 2013, volume 1: Temperature*, NOAA Atlas NESDIS, (Vol. *73*, p. 40).

Lozier, S. M., Bacon, S., Bower, A. S., Cunningham, S. A., Femke de Jong, M., De Steur, L., et al. (2017). Overturning in the Subpolar North Atlantic Program: A new international ocean observing system. *Bulletin of the American Meteorological Society*, *98*(4), 737–752. https://doi.org/10.1175/BAMS-D-16-0057.1

Lumpkin, R., & Speer, K. (2003). Large-scale vertical and horizontal circulation in the North Atlantic Ocean. *Journal of Physical Oceanography*, *33*(9), 1902–1920. https://doi.org/10.1175/1520-0485(2003)033<1902:LVAHCI>2.0.CO;2

Lumpkin, R., & Speer, K. (2007). Global ocean meridional overturning. *Journal of Physical Oceanography*, *37*(10), 2550–2562. https://doi.org/10.1175/JPO3130.1

Macdonald, A. M., & Wunsch, C. (1996). An estimate of global ocean circulation and heat fluxes. *Nature*, *382*(6590), 436–439.

Maltrud, M. E., & McClean, J. L. (2005). An eddy resolving global 1/10 ocean simulation. *Ocean Modelling*, *8*(1–2), 31–54. https://doi.org/10.1016/j.ocemod.2003.12.001

Marshall, J., & Speer, K. (2012). Closure of the meridional overturning circulation through Southern Ocean upwelling. *Nature Geoscience*, *5*(3), 171–180, https://10.1038/ngeo1391

McCarthy, G. D., Smeed, D. A., Johns, W. E., Frajka-Williams, E., Moat, B. I., Rayner, D., et al. (2015). Measuring the Atlantic meridional overturning circulation at 26°N. *Progress in Oceanography*, *130*, 91–111. https://doi.org/10.1016/j.pocean.2014.10.006

McCartney, M. S. (1977). Subantarctic mode water. *Deep Sea Research*, *24*, 103–119.

Meinen, C. S., Speich, S., Piola, A. R., Ansorge, I., Campos, E., Kersalé, M., et al. (2018). Meridional overturning circulation transport variability at 34.5°S during 2009–2017: Baroclinic and barotropic flows and the dueling influence of the boundaries. *Geophysical Research Letters*, *45*, 4180–4188. https://doi.org/10.1029/2018GL077408

Munk, W., & Wunsch, C. (1998). Abyssal recipes II: Energetics of tidal and wind mixing. *Deep Sea Research Part I*, *45*(12), 1977–2010. https://doi.org/10.1016/S0967-0637(98)00070-3

Orsi, A. H., Smethie, W. M., & Bullister, J. L. (2002). On the total input of Antarctic waters to the deep ocean: A preliminary estimate from chlorofluorocarbon measurements. *Journal of Geophysical Research*, *107*(C8), 3122. https://doi.org/10.1029/2001JC000976

Poli, P., Hersbach, H., Dee, D. P., Berrisford, P., Simmons, A. J., Vitart, F., et al. (2016). ERA-20C: An atmospheric reanalysis of the twentieth century. *Journal of Climate*, *29*(11), 4083–4097. https://doi.org/10.1175/JCLI-D-15-0556.1

Sarmiento, J. L., & Bryan, K. (1982). An ocean transport model for the North Atlantic. *Journal of Geophysical Research*, *87*(C1), 394–408. https://doi.org/10.1029/JC087iC01p00394

Sarmiento, J. L., & Le Quere, C. (1996). Oceanic carbon dioxide uptake in a model of century-scale global warming. *Science*, *274*(5291), 1346–1350. https://doi.org/10.1126/science.274.5291.1346

Schmitz, W. J. Jr. (1995). On the interbasin-scale thermohaline circulation. *Reviews of Geophysics*, *33*(2), 151–173. https://doi.org/10.1029/95RG00879

Sloyan, B. M., & Rintoul, S. R. (2001). The Southern Ocean limb of the global deep overturning circulation. *Journal of Physical Oceanography*, *31*(1), 143–173. https://doi.org/10.1175/1520-0485(2001)031<0143:TSOLOT>2.0.CO;2

Smeed, D. A., Josey, S. A., Beaulieu, C., Johns, W. E., Moat, B. I., Frajka-Williams, E., et al. (2018). The North Atlantic Ocean is in a state of reduced overturning. *Geophysical Research Letters*, *45*, 1527–1533. https://doi.org/10.1002/2017GL076350

Smethie, W. M., & Fine, R. (2001). Rates of North Atlantic Deep Water formation calculated from chlorofluorocarbon inventories. *Deep-Sea Research*, *48*, 289–215.

Steele, M., Morley, R., & Ermold, W. (2001). A global ocean hydrography with a high-quality Arctic Ocean. *Journal of Climate*, *14*(9), 2079–2087. https://doi.org/10.1175/1520-0442(2001)014<2079:PAGOHW>2.0.CO;2

Talley, L. D. (1996). Antarctic intermediate water in the South Atlantic. In *The South Atlantic*, (pp. 219–238). Berlin, Heidelberg: Springer. https://doi.org/10.1007/978-3-642-80353-6_11

Talley, L. D. (2003). Shallow, intermediate, and deep overturning components of the global heat budget. *Journal of Physical Oceanography*, *33*(3), 530–560. https://doi.org/10.1175/1520-0485(2003)033<0530:SIADOC>2.0.CO;2

Talley, L. D. (2008). Freshwater transport estimates and the global overturning circulation: Shallow, deep and throughflow components. *Progress in Oceanography*, *78*(4), 257–303. https://doi.org/10.1016/j.pocean.2008.05.001

Talley, L. D. (2013). Closure of the global overturning circulation through the Indian, Pacific, and Southern Oceans: Schematics and transports. *Oceanography*, *26*(1), 80–97. https://doi.org/10.5670/oceanog.2013.07

Toggweiler, J. R., & Samuels, B. (1998). On the ocean's large-scale circulation near the limit of no vertical mixing. *Journal of Physical Oceanography*, *28*(9), 1832–1852. https://doi.org/10.1175/1520-0485(1998)028<1832:OTOSLS>2.0.CO;2

Wang, C., Zhang, L., Lee, S.-K., Wu, L., & Mechoso, C. R. (2014). A global perspective on CMIP5 climate model biases. *Nature Climate Change*, *4*(3), 201–205. https://doi.org/10.1038/nclimate2118

Wright, D. G., Thompson, K. R., & Lu, Y. (2006). Assimilating long-term hydrographic information into an eddy-permitting model of the North Atlantic. *Journal of Geophysical Research*, *111*, C09022. https://doi.org/10.1029/2005JC003200

Zweng, M., Reagan, J. R., Antonov, J. I., Locarnini, R. A., Mishonov, A. V., Boyer, T. P., et al. (2013). In S. Levitus, & A. Mishonov (Eds.), *World Ocean Atlas 2013, volume 2: Salinity*, NOAA Atlas NESDIS, (Vol. *74*, p. 39).